

Journal Pre-proof

Identification of Allosteric Hotspots regulating the ribosomal RNA-binding by Antibiotic Resistance-Confering Erm Methyltransferases

Ruchika Bhujbalrao, Krishna Gavvala, Reman Kumar Singh, Juhi Singh, Christian Boudier, Sutapa Chakrabarti, G. Naresh Patwari, Yves Mély, Ruchi Anand

PII: S0021-9258(22)00650-0

DOI: <https://doi.org/10.1016/j.jbc.2022.102208>

Reference: JBC 102208

To appear in: *Journal of Biological Chemistry*

Received Date: 30 January 2022

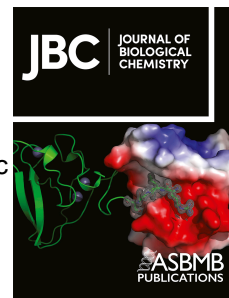
Revised Date: 23 June 2022

Accepted Date: 24 June 2022

Please cite this article as: Bhujbalrao R, Gavvala K, Singh RK, Singh J, Boudier C, Chakrabarti S, Patwari GN, Mély Y, Anand R, Identification of Allosteric Hotspots regulating the ribosomal RNA-binding by Antibiotic Resistance-Confering Erm Methyltransferases, *Journal of Biological Chemistry* (2022), doi: <https://doi.org/10.1016/j.jbc.2022.102208>.

This is a PDF file of an article that has undergone enhancements after acceptance, such as the addition of a cover page and metadata, and formatting for readability, but it is not yet the definitive version of record. This version will undergo additional copyediting, typesetting and review before it is published in its final form, but we are providing this version to give early visibility of the article. Please note that, during the production process, errors may be discovered which could affect the content, and all legal disclaimers that apply to the journal pertain.

© 2022 THE AUTHORS. Published by Elsevier Inc on behalf of American Society for Biochemistry and Molecular Biology.



Identification of Allosteric Hotspots regulating the ribosomal RNA-binding by Antibiotic Resistance-Confering Erm Methyltransferases

Ruchika Bhujbalrao¹, Krishna Gavvala², Reman Kumar Singh¹, Juhi Singh¹ Christian Boudier², Sutapa Chakrabarti³, G. Naresh Patwari^{1*}, Yves Mély^{2,*}, and Ruchi Anand^{1,4,*}

¹ Department of Chemistry, Indian Institute of Technology Bombay, Powai, Mumbai 400076, India

² Laboratoire de Bioimagerie et Pathologies, UMR 7021 CNRS, Université de Strasbourg, Faculté de Pharmacie, 74 Route du Rhin, 67401 Illkirch, France

³ Institute of Chemistry and Biochemistry, Freie Universität Berlin, Takustr. 6, D-14195 Berlin, Germany.

⁴ Wellcome Trust DBT Indian Alliance Senior Fellow

* To whom correspondence should be addressed. Ruchi Anand Tel: 91-25767165; Fax: 91-25767152; Email: ruchi@chem.iitb.ac.in. Correspondence may also be addressed to Yves Mély Tel: +33368854263; Email: yves.mely@unistra.fr and G. Naresh Patwari: Tel 91-25767182 Email: naresh@chem.iitb.ac.in

ABSTRACT

Antibiotic resistance via epigenetic methylation of ribosomal RNA is one of the most prevalent strategies adopted by multi-drug resistant pathogens. The erythromycin-resistance methyltransferase (Erm) methylates rRNA at the conserved A2058 position and imparts resistance to macrolides such as erythromycin. However, the precise mechanism adopted by Erm methyltransferases for locating the target base within a complicated rRNA scaffold remains unclear. Here, we show that a conserved RNA architecture, including specific bulge sites, present more than 15 Å from the reaction center, is key to methylation at the pathogenic site. Using a set of RNA sequences site-specifically labeled by fluorescent nucleotide surrogates, we show that base flipping is a pre-requisite for effective methylation and that distal bases assist in the recognition and flipping at the reaction center. The Erm-RNA complex model revealed that intrinsically flipped-out bases in the RNA serve as a putative anchor point for the Erm. Molecular dynamic simulation studies demonstrated the RNA undergoes a substantial change in conformation to facilitate an effective protein-rRNA handshake. This study highlights the importance of unique architectural features exploited by RNA to impart fidelity to RNA methyltransferases via enabling allosteric crosstalk. Moreover, the distal trigger sites identified here serve as attractive hotspots for the development of combination drug therapy aimed at reversing resistance.

Keywords: Antibiotic resistance; Allosteric cross-talk; RNA Methyltransferases; Ribosome

INTRODUCTION

The alarming increase in antibiotic resistance has posed a serious threat to human health globally (1,2). The persistent evolution and dissemination of resistance genes in pathogenic strains have rendered once easily treatable bacteria resistant to existing antibiotics (3). For curbing the emergence of deadly pathogens one of the promising approaches is to enhance the proficiency of existing antibiotics by inhibiting the resistance machinery itself (4-6). New drug development via this approach necessitates mechanistic interrogation of resistance determinants (7-10). Methylation of nucleobases at select positions of ribosomal RNA is one of the classical hallmarks of antibiotic resistance. The resistance-conferring methyltransferases (Mtases) are known to have distinct specificity for their target base. Despite the advancement in the understanding of how modification in rRNA contributes to resistance, much remains unknown about the molecular mechanism of controlled substrate recognition by Mtases that facilitate this reaction. The DNA Mtases prefer the "bind, and slide" mechanism for locating the target base from a pool of nucleobases, where the Mtase non-specifically binds to the DNA duplex and then scans for the target base by sliding (11). Protein Mtases, on the other hand, have diverse strategies for identifying target amino acids, the most common being the "catch and catalyze" strategy, which is adopted by lysine Mtases (12). This entails globular body recognition which involves conformational

modifications as well as substrate orientation in the methylation catalytic site (12). For the RNA, the tertiary structure is more malleable, and to facilitate function, several bulges and loops, which distort the duplex structure, are present. Hence, the mechanism of target base identification and the algorithm adopted by RNA Mtases is envisioned to be more complex and largely remains elusive.

Since many Mtases that catalyze the exocyclic N⁶ position of adenine have a conserved Rossmann fold and undergo S-adenosyl-L-methionine (SAM) dependent methylation, selective inhibition of these enzymes by targeting active site determinants is difficult. Therefore, a complete understanding of the substrate recognition process and the role played by the flexible architecture of RNA in recognition could potentially aid in the development of novel strategies to selectively inhibit resistance-inducing RNA Mtases. To unravel the mechanism of target recognition in RNA here, we focus on ribosomal methylating erythromycin-resistant methyltransferases (Erm). These enzymes confer resistance to macrolide, streptogramin, and lincosamide (MLS) antibiotics by methylating the N⁶ position of A2058, *Escherichia coli* (*E. coli*) numbering, in the 23S rRNA through a SAM mediated reaction (Scheme 1) (13,14). Resistance occurs as a result of a steric clash between the N⁶ methylated adenine ring and the sugars of the macrolide antibiotics, dislodging them from the protein exit tunnel of the ribosomes (15). Since modification at the A2058 position is associated with reduced translational efficiency, the expression of these Erm is tightly regulated by the translational attenuation mechanism, where onset is triggered only in presence of an antibiotic (16). Erms, possess a highly conserved central Rossmann fold harboring the catalytic domain and a C-terminal region that partakes in ribosomal targeting (13,14). It has been recently established that in Erms, two specific loops at the distal ends of the catalytic domain namely loop1 and loop12 play an important role in RNA recognition (17). While loop1 controls the entry of SAM, it has been implicated that loop12 forms an allosteric pocket that can select for the cognate RNA. Erms faithfully recognize the rRNA loop architecture of helix 73 and exhibit stringent selectivity for their target base (18). This helix lies in the domain V of the ribosome which has been shown as one of the last regions to fold before ribosome biogenesis is complete (19,20). Studies with various truncated versions of helix 73 have revealed that Erms can recognize a substrate mimic which is as small as 27 mer RNA (21). Interestingly, Erms have

been shown to methylate precursor ribosomes and not fully matured ribosomal subunit; hence it is envisioned that a structurally dynamic form of helix 73 is the actual substrate of Erm (20,22). Therefore, in the present study, we aim to decipher the mechanism adopted by RNA Mtases to achieve a high degree of fidelity towards a dynamic and structurally complex RNA architecture. Using a combination of tools, we unravel dynamics and structural changes that facilitate an effective protein-RNA handshake for optimal methylation. The overall goal is to understand how the Rossmann fold harboring sub-class of Mtases, be it protein, DNA, or RNA, harbor a common catalytic mechanism and yet can methylate their respective substrates exclusively. These functional studies represent an important step toward a better understanding of the molecular recognition mechanism of Mtases in general.

RESULTS AND DISCUSSION

Role of 3D RNA scaffold for substrate recognition. The ribosomal Mtases are known to be very specific for their target site. For a better understanding of the substrate profile preferred by Erm Mtases and to identify key bases that participate in recognition, systematic mutagenesis of the minimal 27 mer scaffold adjacent to the A2058 nucleobase was carried out (Figure 1A). The 27-mer substrate mimic was earlier established as a competent substrate of Erm by Douthwaite and coworkers, and Erms has been shown to selectively methylate A2058, therefore it was a logical choice for our study (21). In addition, mFold software and UV melting studies indicates that target RNA adopts hairpin structure (Figure S1). Our experimental results, using 3H-SAM incorporation assays, show that perturbation of selected bases between A2054 and A2062 and its complementary strand C2611 to C2616 has a significant effect on methylation efficiency (Figure 1B). In particular, bulges at U2613-A2614, as well as near position A2054, are essential. Deletion of A2054 results in a loss of activity, while mutations in the U2613-A2614 bulge result in a reduction of activity. Further, shifting the position of the bulges by introducing an extra GC, as in the A1 construct, is detrimental, thereby highlighting the importance of preserving the correct RNA architecture. Corroborating studies by Douthwaite and coworkers have also shown that mutations in out-looped residues such as A2051, C2055, and U2613 also severely affect activity asserting that Erm methylation is not only governed by the conservation of bases adjacent to the methylation site but a long-range communication is at play (23). The

sensitivity of Erm towards the extra helical region indicates that the bulges define the local RNA architecture, which is recognized by Erm as it searches for its cognate RNA. A minimal effect on RNA methylation was observed for the synthetically created A2 version, where an extra GC was introduced at G2053, before the extra-helical bulge region. Thus, bases upstream of the bulge do not partake in substrate recognition (Figure 1B). Recent studies identifying Erm's minimal substrates also revealed that secondary features of RNA are critical for recognition (24). Thus, the biochemical and MALDI (Figure 1 and Figure S2) results presented herein in corroboration with previous reports hint that the specificity is achieved via a proper structural fit of the RNA with Erm with the conserved bulge region, which is 15 Å from the methylation site, playing a key role in recognition.

Mechanism of RNA methylation at the target site. RNA exhibits structural plasticity and the recognition sequence is not a simple duplex. Therefore, to explore the importance of the 3D architecture, site-specific fluorescent nucleobase surrogates 2-aminopurine (2Ap) and thienoguanosine (thG) were introduced within the RNA template (RT) (Figure S3). The aim was to delineate the possibility of the distal bulges acting as hot spots that help induce global motion leading to the appropriate orientation of the target base, A2058, or if the template is preorganized and Erm methylates its target via minimal perturbation of the presented architecture. The 2Ap was introduced at nucleobase positions 2054, 2058, 2059, and 2614 henceforth referred to as 2Ap2054, 2Ap2058, 2Ap2059, 2Ap2614 respectively and thG was incorporated at positions 2057 and 2061 referred to as thG2057 and thG2061 respectively. Both of these fluorescent nucleobase analogs chosen for the study have been widely used in several systems and have been established as excellent environmental-sensitive probes used to monitor the conformational dynamics of nucleic acids (25-29). These nucleobase surrogates cause minimal perturbation in the integrity of the nucleic acid structures and show enhanced fluorescence signals upon de-stacking. The substitution by nucleobase surrogates does not significantly affect the RNA architecture, which was measured by the methylation assay, with the exception of 2Ap at the A2058 position (Figure S4A). Further, the binding affinity of ErmS for the labeled constructs was assessed by a change in fluorescence anisotropy with increasing concentration of enzyme, assuming a 1:1 binding model. The K_d values for all labeled

RNAs were found to agree with the value obtained by filter binding assay with the unmodified construct (Figure 2, S4B) indicating that fluorophore-labeled RNA constructs can be recognized by ErmS. The comparatively higher K_d value for 2Ap2058 was expected as due to the replacement of A2058 by 2Ap as the enzyme is unable to orient the target base in a conformation favorable for catalysis. Moreover, in the presence of SAM, there is a marginal change in K_d observed for the 2Ap2058 position, which suggests that local restructuring of the target base site is induced in the presence of SAM. No significant change in K_d was observed for remaining labeled RNA in presence of a cofactor. To delve deeper into the mechanism of methylation, the fluorescence response of the 2Ap2058 RNA template in the presence and absence of Erm was gauged. When increasing amounts of ErmS were titrated to a fixed concentration of 2Ap2058, fluorescence enhancement was observed. Figure 3A, S4C and S5A show that the addition of a 5-fold molar excess of Erm resulted in a significant increase in the fluorescence signal. The Erm enzyme by itself showed negligible fluorescence in our experimental conditions. Hence, the enhancement in the fluorescence signal detected can solely be ascribed to changes in the fluorophore environment. This increase in fluorescence intensity is akin to what has been observed earlier in DNA Mtases, where a base flipping of the target base results in enhanced fluorescence as the base gets buried into the protein pocket (11,30). Since DNA Mtases also harbor a Rossmann fold SAM-dependent Mtase domain, we envision a similar mode of recognition is adopted by RNA Mtases. As the A2058 in h73 (Figure S3A) is loosely stacked with its flanking bases A2059 and G2056, base flipping should only result in a modest increase in fluorescence. In the Erm-RNA complex, the net fluorescence change observed is a combination of quenching of 2Ap at 2058 due to interaction with active site residues 101-NPPY-104 as well as an increase due to base flipping which explains the relatively limited change in intensity of the signal.

To confirm the attribution of the observed fluorescence change to base flipping, stopped-flow kinetic studies were carried out. When the 2Ap2058 construct was rapidly mixed with ErmS, a fast fluorescence component increases in the millisecond range, followed by a slower component in the seconds range, was observed (Figure 3F). By repeating this reaction at several protein concentrations, the slower phase could be fitted to a double-exponential equation, using kinetic rate constants that were

independent of the protein concentration (data not shown). This suggests that the slow component describes two first-order reactions, and hence, the data could be fitted with a three-step model similar to the base flipping reaction of *E. coli* Dam DNA-(adenine-N⁶)-Mtases (Scheme 2) (30). The Dam Mtase is a well-studied DNA Mtase that acts on exocyclic N⁶ adenine, similar to Erm. Moreover, the active site residues are highly conserved between both families of proteins, and hence is a good comparative system to use. Based on the *E. coli* Dam Mtase DNA binding model (31,32), the fast initial step corresponds to a "bind-and-slide" mechanism, followed by the fast fluorescence increase due to base flipping reaction (governed by k_2 and k_{-2} rate constants) and the subsequent rearrangement of 2Ap in the active site of the enzyme (governed by k_3 and k_{-3} rate constants) as shown in Scheme 2. The stopped-flow kinetic data was fitted to this model, using Dynafit numerical solving software (33), which can be used in the non-pseudo-first order conditions of our experiments and does not make any assumption on the relative values of the rate constants in the selected kinetic model. Using this model, the association rate constant $k_1 = 5.0 \pm 0.4 \times 10^6 \text{ M}^{-1} \text{ s}^{-1}$ and dissociation rate constant $k_{-1} = 32 \pm 2 \text{ s}^{-1}$ as well as the kinetics of the final conformational changes ($k_3 = 0.19 \pm 0.01 \text{ s}^{-1}$) were found to be in good agreement with the rate constants reported for other DNA Mtases (Table 1) (30,34,35). However, the kinetics of 2Ap flipping ($k_2 = 3.4 \pm 0.5 \text{ s}^{-1}$) was significantly slower than DNA Mtases (30,34) but similar to that observed for only tRNA Mtase (11,36). Finally, in line with the kinetics obtained with *E. coli* DNA Mtase (30), our fits and simulations suggest that base flipping of the target base occurs in Erm Mtases. The rate constants k_2 and k_{-2} govern the back reactions of base flipping, and the subsequent conformational changes are negligibly small.

To understand the potential role of the cofactor SAM in base flipping, stopped-flow kinetics was monitored in the presence of the SAM analog, sinefungin (Figure 3F). This analog led to a substantial increase in the value of k_1 , but a marginal change in the k_2 value (Table 1). The k_1 could not be precisely determined, because a large part of the fluorescence increase occurred during the dead time (2.7 ms) of the instrument. A similar increase in the k_1 value with a nominal change in the value of k_2 in the presence of SAM analogs was previously reported for EcoRV DNA Mtase (35). The substantial fluorescence increase within the first seconds was followed by a slow and

moderate fluorescence decrease. This slow decrease at a later time point is attributed to the stacking of adenine with the active site Tyr104 that is induced upon SAM binding. A similar scenario was observed for Dam DNA Mtase when stopped-flow kinetics were performed in the presence of a cofactor (30). Thus, it appears that the local mechanism of identification of the target base at the active site is analogous for both DNA and RNA N⁶ adenine Mtases. It's intriguing to note that these Mtases are substrate-specific; hence, apart from a good fit with the immediate environment, the second layer of recognition appears to be the deciding factor in maintaining catalytic stringency.

Allosteric control of methylation. Since RNA Mtases selectively methylate certain RNA scaffolds and have a high degree of fidelity, efforts were made to identify the bases involved in imparting specificity of recognition. To understand the structural basis of the selection of the methylation site, RNA templates with fluorophores at locations other than A2058 were analyzed. Fluorescence studies showed limited changes in the fluorescence signal for immediate neighbors of A2058, indicating that the local environment of A2059 and G2057 is marginally impacted by the base flip (Figures S5B S5E, and Figure 3D). In helix 73, A2059 is loosely stacked with adjacent base A2060 and mostly solvent-exposed, which also explains for lack of change in fluorescence due to base flipping. In contrast, the distal bulge sites that have been ascertained in the scintillation experiments to be paramount for the activity positions 2Ap2054, and 2Ap2614, show a dramatic increase in fluorescence upon interaction with Erm (Figure 3B, 3C and Figures S5C, S5D). In both cases, significant enhancement, 5 to 3.5 fold, respectively, for 2Ap2054, and 2Ap2614 sites indicates that the presence of ErmS has significantly influenced the bulge region and indicates that protein induces a significant rearrangement of the proximal environment around the bulge site. Monitoring fluorescence via the reporter probe thG2061 at the other end of the recognition sequence shows about 8 nm blue shift, which is indicative of an increase in hydrophobicity in its surroundings upon Erm binding (Figures 3E and Figure S5F). These differences in spectra at both the bulge sites as well as at other distal positions are clear indicators that reorganization of the RNA occurs to facilitate the protein-RNA handshake. As the most significant effect was detected at the bulge position, A2054, this construct was subjected to further investigation by stopped-flow (Figure 3F and Supplementary Figure S6). The rate constants obtained for the 2Ap2054 kinetic

traces both in the absence and presence of sinefungin (Table 1) were very similar to those observed with 2Ap2058, indicating that the conformational changes that occur at the two positions are concomitant. Taken together, our fluorescence data suggest that the rRNA bulges undergo dynamic conformational changes upon Erm binding and facilitate A2058 flipping via a long-range orchestrated motion.

Insights into conformation dynamics. To understand the molecular basis for the observed experimental results and to comprehend how these bulge sites play a crucial role in mediating long-distance cross-talk, we constructed a model of RNA-ErmC' complex. The ErmC' (PDB ID 1QAM) was used as a starting protein conformation and for the RNA two basic templates were created and several variations were introduced in these two templates. The first template is the modeled structure of RNA in solution, which was obtained by optimizing the free energy. The modeled RNA shows a hairpin conformation in the solution (Figure 4A and Figure S7A), which was confirmed by folding and unfolding studies (Figure S7C). The second template was a mini-RNA extracted from the crystal structure of the 50S ribosomal RNA. The RNA templates were docked on the protein with HADDOCK using the active-site analysis, *vide-infra*, wherein the protein residues 100-104 interact with the A2058 base of the RNA, and MD simulations were carried out for 200 ns to obtain a stable structure of RNA-Protein complex (Figure 4A). In the model, RNA interacts with the positively charged interface of the Erm consistent with the model obtained by Goh, B. et al. (37)

In order to gauge the most plausible interaction interface, multiple MD simulations were carried out with interacting bases in various conformations. For instance, the bases in bulges (U2613, A2614, and C2055) were either kept in flipped-in or flipped-out states so as to see how various structures evolve during the simulations. The dynamic behavior of the template RNA and the impact on the pertinent base conformations on A2058 flipping was evaluated (Table S1). It was observed, at 25 °C, for simulations with 50S ribosomal substrates that A2058 does not spontaneously flip out on its own in a 200 ns time period, implying the presence of a higher barrier. Therefore, metadynamics simulations using the two dihedral angles (see Figure S8 in the SI for the definition of dihedral angles) as reaction coordinates were carried out in which the bases A2058 and U2613 are flipped out as the reaction progresses, and are represented by dihedral angles $\chi-1$ and $\chi-2$, respectively. The

consequent free energy surface of base flipping and the barrier associated with the minimum free energy path for the base-flipping process is 13 kcal mol⁻¹ in the presence of the protein. Alternatively, simulations performed at growth temperature (37 °C) showed progression of the base flipping for A2058 in a 1 μ s time scale. The metadynamics simulations reveal that A2058 flips and inserts itself into the active site pocket lined by the conserved NIPY motif, similar to that observed for DNA Mtases. The insertion of A2058 facilitates the flipping of U2613. Figures 4E and 4F show the comparison of MD snapshot for RNA-Erm complex with the crystal structure view of the DNA Mtase highlighting the analogous geometry of recognition in these classes of enzymes.

Further, the conformational change was monitored by the changes in the inter-base distances in the unbound RNA, at the start (0 ns) of simulation and 140 ns by the distance map plotted using RNAmapping2D (Figure S9). The distance matrix revealed that residues close to A2058 between C2055 and A2060 undergo significant displacement to accommodate the base flipping event (Figure 4C). Though no major change in distance was observed for the A2054-U2615 base pair, the stacking interactions with its neighboring bases were disrupted during simulation (Figure 5A & 5B). The binding of U2613 with the loop 12 of the Erm triggers reorientation in the residues flanking A2054. The distance between A2054 and C2055 increases (Figure 4C) whereas A2614 rotates and moves away from U2615. Both A2054 and A2614 residues experience de-stacking in the presence of Erm which can explain for increase in fluorescence signal, the effects being more predominant for the A2614 position. On the other hand, G2057 remained stacked by surrounding bases throughout the simulation and distance between G2057-C2611 did not change substantially (Figure S11). The trend observed in the simulations is in close agreement with the fluorescence studies, therefore we believe that the simulations provide a reasonable estimate of the protein-RNA interactions. The fluorescence enhancement at 2058 can be rationalized by base flipping whereas, changes in 2054 and 2614 can be due to changes in the environment around these bases that are induced by Erm. Moreover, the changes corresponding to the 2057 and 2056 positions are only marginal, which are in line with the corresponding fluorescence measurements.

Analysis of the various snapshots from the trajectory reveal a long-distance communication where RNA is anchored to the

protein via one of its faces laterally across the length of the protein (Figure 4B). The RNA is tethered at one end via base A2060 near the N-terminal side of Erm. The other end is tethered via U2613 which interacts with a positively charged surface created at the interface of the Rossmann fold of Mtase domain and the C-terminal domain of ErmC' (Figure 5C). This region of Erm forms a shallow pocket nested between loop12 and the C-terminal domain where the flipped base U2613 inserts itself (Figure 5D). Therefore, these two loops act as an anchor for target RNA. Combining insights from MD simulations and fluorescence measurements, we conclude that RNA first locks onto the Erm via the extra helical bulge regions and concomitantly forms contacts with the key Erm recognition elements, loop 1 and loop 12. Simultaneously, the overall RNA scaffold starts to open up and the hydrogen-bonding interactions between the central base pairs weaken. The base stacking interaction of A2054 is disrupted, and this orchestrates a rearrangement that distorts the phosphodiester backbone providing the exit route for the flip of the target base, A2058, into the active site. Thus, perturbation around A2054, and regions surrounding the bulges, 15 Å away, bring the target base close to the active site of Erm. In this respect, the three steps of the fluorescence kinetics observed with 2Ap2054 could be logically interpreted in the following way. The first step governed by k_1 and k_{-1} is common to the first step of 2Ap2058 and corresponds to the nonspecific binding of Erm to the RNA and in locating the target site. The second step governed by k_2 is concurrent with the base flipping of A2058 and corresponds to the motion of A2054 and the loss of its base stacking interactions. The final step, governed by k_3 , might be attributed to the slow conformational adjustments needed to allow the optimal positioning of A2058 in the active site pocket. The interface thus mimics a lock and key scenario where the bulges act as hot spots to facilitate optimal recognition and induce a dynamic restructuring across the length of the RNA sequence.

Perspectives into RNA methylation. Post-translational methylation, both at the nucleic acid and protein level, is a pivotal epigenetic modification required for fine-tuning various vital processes like biogenesis, cellular signaling, virulence, etc. (38-41). For instance, strategic methylation at specific RNA splice variants (42,43) controls gene expression. Likewise, in chromatin remodeling, methylation is introduced at select lysine/arginine residues of histones and silences transcription (44). Bacteria have exploited the power of this

methylation mark by selectively introducing it at various positions within the ribosome to achieve resistance to several drugs (15,45). It is intriguing to note as to how various Mtases harbor similar catalytic residues yet, each enzyme methylates its target site with a high degree of fidelity. This emphasizes the fact that the targeting determinants potentially lie outside the catalytic region. Analyzing various types of methylation marks such as protein Mtases, like K27 lysine Mtase, it becomes apparent that this sub-class achieves specificity by the formation of a multiprotein complex (e.g., polycomb complex) that imparts selectivity (46,47). In the case of DNA Mtases, specific DNA binding domains search for the correct target sequence and present it to the Mtase domain (48,49). Here, we have established that in Erm Mtases, the mechanism operates via long-distance allosteric modulation. In the case of Erm Mtase, the out-looped bases are recognized, and a major reorganization is initiated distally (about 15 Å away) to facilitate appropriate conformational change at the target site. The crucial role played by bulge sites is apparent as in the absence of these extrahelical elements, Erm is unable to methylate its target base. Moreover, the position of the bulges within the target sequence is programmed; any misalignment of the bulge site results in the abolishment of methylation. Thus, methylation at the target site is strictly controlled by the 3D architecture of the RNA, and is intolerant to perturbation.

In this work, we have shown that a local mechanism of RNA methylation is akin to "bind and slide" as observed for DNA Mtases is operative in Erm, wherein base flipping is a fundamental prerequisite for methylation. However, in RNA Mtases to facilitate the base flipping, reorganization of the distal extra helical region is a prerequisite. This suggests that intermittent hopping, in conjunction with the "bind and slide" approach, is used to overcome structural extrusions by RNA Mtases when tracking the target site. Many known base flipping enzymes anchor onto the target site with the help of extra helical bases. For example, the structure of the RumA-RNA complex showed flipping of a secondary base other than the target base (U1939) which stabilizes the cofactor and helps in the anchoring of protein to the substrate like Erm (Figure 6B & 6E). In the case of RumA, the entire RNA backbone in the vicinity of the target base undergoes rearrangement to fill the void created by the flipping of the two bases (50). Base flipping is an energetically demanding process, hence several base flipping enzymes resort to rearrangement in the DNA/RNA

backbone structure similar to that of the Erm-RNA complex to lower the activation energy barrier. In uracil Mtases TrmA (similar to RumA), the conformation of the T-arm of the tRNA bound to the protein is different from the native tRNA due to the destabilization of surrounding bases (51). Another well-studied methylase Nsun6 shows a similar flipping of adjacent bases to facilitate the binding of a target base in the active site (52) (Figure 6C). Similarly, DNA Mtases and ADAR deaminases which also resort to the base flipping mechanism for recognition of substrate, flipping of neighboring bases, and separation/opening up of the phosphodiester backbone are proposed to help inversion of target base (53). It was recently shown, in a structure of KsgA, a structural homolog of Erm, in a complex with the 30S ribosome, that in addition to the target base A1519, a neighboring base G1516 flips, which aids in proper protein anchoring (Figure 6F)(54,55). These structures suggest that Mtases uses allosteric sites for recognition of RNA architecture. A set of signature interactions that are conserved for a particular RNA-protein set but differ for different Mtases helps create a diverse set of RNA-Mtases interfaces that impart its selectivity for a cognate pair.

To conclude, this work demonstrates how naturally programmed bulges in the rRNA sequence govern the complicated algorithm of recognition by Mtases. The allosteric sites identified here provide lucrative avenues for drug design. Instead of targeting the common conserved Mtase catalytic site that has the potential to generate off-target effects, inhibitors can be developed for these distal bulge sites. Freezing dynamics of the specific identified out-loop region will impede protein interaction and block methylation, thereby reversing resistance.

EXPERIMENTAL PROCEDURES

The fluorescent-labeled 27mer RNA sequence (GGCAAGACGGAAAGACCCCUAUCUGCC) with 2-aminopurine (2Ap) at A2054, A2058, A2059 position were synthesized at a 1.0 μ mol scale by IBA GmbH Nucleic Acids Product Supply (Göttingen, Germany) and at A2614 position were procured from Integrated DNA technologies. RNA sequence with thienoguanosine (thG) at G2057 and G2061 were obtained from TriLink Biotechnologies (U.S.A.). The un-labeled RNA constructs were synthesized using the in-vitro transcription method (56).

Cloning and purification of ErmS

Dimethyltransferase (*TlrA*, *ErmS*) gene was cloned from *Streptomyces fradiae* (gift from Prof. Eric Cundliffe, University of Leicester) into the modified pET expression vector using primers having restriction sites NdeI and XhoI. The recombinant *ErmS* clone was transformed into *Escherichia coli* BL21 (DE3) Rosetta cells, overexpressed with 1 mM Isopropyl- β -D-thiogalactopyranoside at 16 °C for 16 h and subsequently purified using ion-exchange chromatography. Briefly, the cell pellet was resuspended in lysis buffer (50 mM HEPES and 1 X protease inhibitor, pH 8.0). The cells were further disrupted by sonication (10 pulses, 20% Amplitude) and centrifuged at 14,000 rpm for 45 min. The supernatant was mixed with pre-equilibrated SP-sepharose beads (Sigma-Aldrich) and incubated on a rocker for 1 h at 4 °C. Beads were then extensively washed with wash buffer (50 mM HEPES pH 8.0). The proteins were eluted with increasing concentrations of NaCl (100 mM -1 M) and detected in collected fractions using 15% SDS-polyacrylamide gels with Coomassie blue staining. The *ErmS* protein was eluted at 500 mM salt concentration. The pure protein fractions were further desalted using an Econo-Pac 10DG (Bio-Rad, CA, USA) column pre-equilibrated with a desalting buffer (20 mM HEPES pH 7.5, 100 mM NaCl). The protein was further concentrated up to 6 mg/mL, as determined by the Bradford assay using bovine serum albumin as a standard, and then flash-frozen in liquid N₂ and stored at -80 °C until further use.

Filter binding assay

The RNA-binding properties of Erm were determined using a 27mer RNA oligonucleotide synthesized using the in vitro transcription protocol (56). Briefly, the oligonucleotide substrate was labeled radioactively using adenosine-5 [γ -³²P] triphosphate and T4 polynucleotide kinase. RNA (20 nM) was titrated with increasing concentrations (0.5 -10 μ M) of Erm in binding buffer [50 mM HEPES, pH 7.5, 40 mM KCl, 4 mM Mg (OAc)₂, 10 mM DTT, 1 mM EDTA, 0.2 mg/L BSA] with the addition of 1 U of RNasin per reaction mixture. Binding reactions were carried out in a reaction volume of 10 μ L for 20 min at 37°C. Nitrocellulose filter sheets (pore size 0.22 mm) were pre-incubated for 1 h in binding buffer. The reaction mixture was then blotted onto pre-soaked filters, followed by washing with the binding buffer to eliminate non-specific binding. After drying, the filters were exposed overnight to the intensifying screen and the amounts of bound complexes were determined using a

Phosphoimager Storm625 (GE Healthcare, WI, USA). Experiments were repeated in triplicate.

Methylation assay

The wild-type 27mer RNA and modified RNA constructs were annealed by a temperature cycle where the samples were heated at 90 °C for 1 min and then cooled slowly to room temperature. The reaction was carried out in methylation buffer [50 mM HEPES (pH 7.5), 40 mM KCl, 4 mM MgCl₂, 10 mM DTT] containing 4 μM of rRNA, 0.5 μM Erm, 0.2 μM (3H)-S-adenosyl-l-methionine [(methyl-3H) AdoMet, 16 Ci/mmol), and 1 U of RNasin in a total reaction volume of 50 μL and incubated at 37 °C. The reaction was stopped by the addition of 2.5 mM ammonium acetate followed by ethanol precipitation. RNA pellets were then blotted on Nylon-66 filters pre-soaked in methylation buffer, further washed to remove non-specific binding. Radioactivity was recorded using a scintillation counter (Tri-Carb B2810TR; PerkinElmer, USA). Experiments were performed in triplicate.

Steady-state fluorescence

Fluorescence spectra of the complexes of ErmS and fluorescently labeled RNA were recorded at 20 °C on a FluoroLog spectrofluorometer (Jobin Yvon) equipped with a thermostated cell compartment. The excitation wavelength was set at 315 nm for 2Ap-labelled RNA and 350 nm for thG-labeled constructs. The fluorescence emission was recorded from 325 to 650 nm for 2-aminopurine and from 365 to 600 nm for thienoguanosine. Spectra were corrected for buffer fluorescence, protein fluorescence, lamp fluctuations, and detector spectral sensitivity. For experiments involving 2Ap2058, 2Ap2059 2Ap2054, and 2Ap2614 constructs, the concentration of RNA was 2 μM. For the other RNAs, 0.5 μM RNA concentration was used for steady-state fluorescence studies. Prior to the recording of spectra, Erm and RNA were incubated for 1 min to reach equilibrium. Steady-state anisotropy measurements in the presence and absence of SAM were performed on the same instrument. The excitation wavelengths for 2Ap- and thG-labelled constructs were as mentioned previously. The fluorescence anisotropy was measured at 365 nm and 460 nm, respectively. Anisotropy values were obtained by averaging 10 measurements. The affinity constants for Erm were determined by fitting the fluorescence anisotropy changes using the following equation 1:

$$r = \frac{vRr_t - r_d(v-1)}{1 + Rv - v}$$

$$v = \frac{\left(\frac{1}{K_a} + nL_t + P_t\right) - \sqrt{\left(\frac{1}{K_a} + nL_t + P_t\right)^2 - 4nP_tL_t}}{2L_t}$$

where r and r_t are the anisotropy values at a given, and a saturating protein concentration, respectively, and r_d is the anisotropy in the absence of protein. R is the ratio of the quantum yields of the bound to free forms, K_a is the apparent affinity constant, v is the fraction of bound Erm, P_t and L_t are the concentrations of ErmS and 27 mer labeled RNA, respectively, and n is the number of Erm proteins bound per molecule of RNA (11).

Stopped-flow measurements

The kinetics of Erm binding to the RNA constructs was monitored using a stopped-flow apparatus (SFM-3, Bio-Logic, Claix, France) equipped with a temperature-controlled circulating water bath. The excitation wavelength for 2Ap was 315 nm (same as fluorescence measurements), and the fluorescence intensity above 320 nm was recorded with long-pass filters. The dead time of the setup was 2.7 ms. The kinetics of binding was recorded by the fast mixing of RNA and Erm alone or in complex with Sinefungin (1 mM). The final concentration of labeled RNA was 1.0 μM, and the concentration of protein was chosen to saturate RNA. Background signal was obtained by mixing RNA with the buffer under the same conditions. All the reactions were performed in the methylation buffer. Up to five datasets were collected and averaged for each condition. The averaged traces were collectively analyzed with the numerical solving software Dynafit to obtain the kinetic rate constants of scheme 2.

Molecular dynamics simulations

The molecular dynamics (MD) simulations were carried out in double-precision Gromacs 2020.2 (57) patched with plumed-2.6 (58) for the simulations and free energy calculations. To begin with, the solution conformation of the GGCAAGACGGAAAGACCCCUAUCUGCC RNA sequence was modeled wherein a single-stranded RNA sequence was generated and MD simulations were carried out to converge on to the stable structure. Further, the hairpin conformation of this sequence for the ribosome (59) was also modeled for stability. The two methods converged onto an almost identical structure with an average RMS deviation of 2.1 Å. Modeling of the RNA protein complex was carried out using High Ambiguity-Driven protein-protein DOCKing (HADDOCK 2.2)

server to dock the RNA on protein. The protein (ErmC') conformation is taken from the protein data bank (PDB ID 1QAM) and the modeled RNA conformation, *vide supra*, was taken. The active site residues for ErmC', amino acids 101–104, and the rRNA position A2058 were fixed during docking. Docking of ErmC' was performed using the Easy interface option available on the HADDOCK server, which uses simulated annealing and a steepest-descent technique for interaction energy minimization. The lowest energy model was used for molecular dynamics studies and further analysis. The dynamics and the free energy landscape of the single-stranded RNA and RNA bound to protein were explored by defining an appropriate reaction coordinate in each case. For the single-stranded RNA, the reaction coordinate is the end-to-end distance, while for the RNA bound to protein, the reaction coordinate involved base flipping which was characterized by the base1-phosphate1-phosphate2-base2 dihedral angle (see the Methodology in the supporting information for details). The minimum energy path along these two reaction coordinates was sampled using Well-Tempered Metadynamics Simulations in combination with the sum_hills module of plumed which was used to calculate the unbiased population along the reaction coordinate and its free energy (60).

DATA AVAILABILITY STATEMENT

The authors confirm that the data supporting the findings of this study are available within the article and its supplementary information. The raw data files are available upon request.

SUPPORTING INFORMATION

This article contains supporting information

ACKNOWLEDGEMENT

We thank the SpaceTime-2 supercomputing facility and scintillation facility at IIT Bombay. The support and the resources provided by 'PARAM Brahma Facility' under the National Supercomputing Mission, Government of India at the Indian Institute of Science Education and Research (IISER) Pune are gratefully acknowledged. We also thank Mr. Amol Tagad for his help with MD simulations.

AUTHOR CREDIT STATEMENT

Ruchika Bhujbalrao: Visualisation, Investigation, Methodology **Krishna Gavvala:**

Investigation (fluorescence experiments) **Reman Kumar Singh:** Investigation (molecular dynamic studies) **Juhi Singh** (UV melting and MALDI) **Christian Boudier:** Formal analysis **Sutapa Chakrabarti:** Writing- Reviewing and Editing **G. Naresh Patwari:** Writing- Reviewing and Editing **Yves Mély:** Supervision, Resources, Writing - Original Draft **Ruchi Anand:** Conceptualization, Supervision, Resources, Writing - Original Draft

FUNDING

This work was funded by Wellcome Trust Senior Fellowship by the DBT India alliance (grant number IA/S/19/1/504293) and the Indo-German program sponsored by UGC. KG was supported by the Fondation pour la Recherche Médicale. YM is grateful to the Institut Universitaire de France (IUF) for support and for providing additional time to be dedicated to research. This work was also supported by the Agence Nationale de la Recherche (ANR SMFLUONA), the Labex NIE and the Centre National pour la Recherche Scientifique (CNRS). Funding for open access charge: Wellcome Trust Senior Fellowship by DBT India alliance.

CONFLICT OF INTEREST

The authors declare no competing financial interests

REFERENCES

1. Aslam, B., Wang, W., Arshad, M. I., Khurshid, M., Muzammil, S., Rasool, M. H., Nisar, M. A., Alvi, R. F., Aslam, M. A., Qamar, M. U., Salamat, M. K. F., and Baloch, Z. (2018) Antibiotic resistance: a rundown of a global crisis. *Infect Drug Resist* **11**, 1645-1658
2. Bragginton, E. C. P., L. J. V. (2014). *Lancet Infect. Dis* **14**
3. Li, B., and Webster, T. J. (2018) Bacteria antibiotic resistance: New challenges and opportunities for implant-associated orthopedic infections. *J Orthop Res* **36**, 22-32
4. Davies, J., and Davies, D. (2010) Origins and Evolution of Antibiotic Resistance. *Microbiology and Molecular Biology Reviews* : *MMBR* **74**, 417-433
5. Wright, G. D. (2007) The antibiotic resistome: the nexus of chemical and genetic diversity. *Nat Rev Micro* **5**, 175-186

6. Wright, G. D., and Sutherland, A. D. (2007) New strategies for combating multidrug-resistant bacteria. *Trends in Molecular Medicine* **13**, 260-267
7. Eumkeb, G., Sakdarat, S., and Siriwong, S. (2010) Reversing β -lactam antibiotic resistance of *Staphylococcus aureus* with galangin from *Alpinia officinarum* Hance and synergism with ceftazidime. *Phytomedicine* **18**, 40-45
8. Hajduk, P. J., Dinges, J., Schkeryantz, J. M., Janowick, D., Kaminski, M., Tufano, M., Augeri, D. J., Petros, A., Nienaber, V., Zhong, P., Hammond, R., Coen, M., Beutel, B., Katz, L., and Fesik, S. W. (1999) Novel Inhibitors of Erm Methyltransferases from NMR and Parallel Synthesis. *Journal of Medicinal Chemistry* **42**, 3852-3859
9. Sarah, C. (2017) Reversing resistance. *Nature Reviews Drug Discovery* **16**, 314
10. Wright, G. D. (2000) Resisting resistance: new chemical strategies for battling superbugs. *Chemistry & Biology* **7**, R127-R132
11. Kilin, V., Gavvala, K., Barthes, N. P. F., Michel, B. Y., Shin, D., Boudier, C., Mauffret, O., Yashchuk, V., Mousli, M., Ruff, M., Granger, F., Eiler, S., Bronner, C., Tor, Y., Burger, A., and Mély, Y. (2017) Dynamics of Methylated Cytosine Flipping by UHRF1. *Journal of the American Chemical Society* **139**, 2520-2528
12. Kuiper, E. G., Dey, D., LaMore, P. A., Owings, J. P., Prezioso, S. M., Goldberg, J. B., and Conn, G. L. (2019) Substrate recognition by the *Pseudomonas aeruginosa* EF-Tu-modifying methyltransferase EftM. *J Biol Chem* **294**, 20109-20121
13. Schluckebier, G., Zhong, P., Stewart, K. D., Kavanaugh, T. J., and Abad-Zapatero, C. (1999) The 2.2 Å... structure of the rRNA methyltransferase ErmC' and its complexes with cofactor and cofactor analogs: implications for the reaction mechanism¹. *Journal of Molecular Biology* **289**, 277-291
14. Yu, L., Petros, A. M., Schnuchel, A., Zhong, P., Severin, J. M., Walter, K., Holzman, T. F., and Fesik, S. W. (1997) Solution structure of an rRNA methyltransferase (ErmAM) that confers macrolide-lincosamide-streptogramin antibiotic resistance. *Nature Structural Biology* **4**, 483
15. Auerbach, T., Bashan, A., and Yonath, A. (2004) Ribosomal antibiotics: structural basis for resistance, synergism and selectivity. *Trends in Biotechnology* **22**, 570-576
16. Dzyubak, E., and Yap, M. N. (2016) The Expression of Antibiotic Resistance Methyltransferase Correlates with mRNA Stability Independently of Ribosome Stalling. *Antimicrob Agents Chemother* **60**, 7178-7188
17. Bhujbalrao, R., and Anand, R. (2019) Deciphering Determinants in Ribosomal Methyltransferases That Confer Antimicrobial Resistance. *Journal of the American Chemical Society* **141**, 1425
18. Kovalic, D., Giannattasio, R. B., Jin, H. J., and Weisblum, B. (1994) 23S rRNA domain V, a fragment that can be specifically methylated in vitro by the ErmSF (TlrA) methyltransferase. *Journal of Bacteriology* **176**, 6992-6998
19. Davis, J. H., and Williamson, J. R. (2017) Structure and dynamics of bacterial ribosome biogenesis. *Philos Trans R Soc Lond B Biol Sci* **372**, 20160181
20. Pokkunuri, I., and Champney, W. S. (2007) Characteristics of a 50S ribosomal subunit precursor particle as a substrate for ermE methyltransferase activity and erythromycin binding in *Staphylococcus aureus*. *RNA Biology* **4**, 147-153
21. Hansen, L. H., Lobedanz, S., Douthwaite, S., Arar, K., Wengel, J., Kirpekar, F., and Vester, B. (2011) Minimal Substrate Features for Erm Methyltransferases Defined by Using a Combinatorial Oligonucleotide Library. *ChemBioChem* **12**, 610-614
22. Champney, W. S., Chittum, H. S., and Tober, C. L. (2003) A 50S Ribosomal Subunit Precursor Particle Is a Substrate for the ErmC Methyltransferase in *Staphylococcus aureus* Cells. *Current Microbiology* **46**, 0453-0460
23. Vester, B., Nielsen, A. K., Hansen, L. H., and Douthwaite, S. (1998) ErmE methyltransferase recognition elements in RNA substrates¹. *Journal of Molecular Biology* **282**, 255-264
24. Lee Hak, J., Park Young, I., and Jin Hyung, J. Plausible Minimal Substrate for Erm

- Protein. *Antimicrob Agents Chemother* **64**, e00023-00020
25. Shin, D., Sinkeldam, R. W., and Tor, Y. (2011) Emissive RNA Alphabet. *Journal of the American Chemical Society* **133**, 14912-14915
26. Sholokh, M., Improta, R., Mori, M., Sharma, R., Kenfack, C., Shin, D., Voltz, K., Stote, R. H., Zaporozhets, O. A., Botta, M., Tor, Y., and Mély, Y. (2016) Tautomers of a Fluorescent G Surrogate and Their Distinct Photophysics Provide Additional Information Channels. *Angewandte Chemie* **128**, 8106-8110
27. Sholokh, M., Sharma, R., Shin, D., Das, R., Zaporozhets, O. A., Tor, Y., and Mély, Y. (2015) Conquering 2-Aminopurine's Deficiencies: Highly Emissive Isomorphous Guanosine Surrogate Faithfully Monitors Guanosine Conformation and Dynamics in DNA. *Journal of the American Chemical Society* **137**, 3185-3188
28. Jones, A. C., and Neely, R. K. (2015) 2-aminopurine as a fluorescent probe of DNA conformation and the DNA–enzyme interface. *Quarterly Reviews of Biophysics* **48**, 244-279
29. Dziuba, D., Didier, P., Ciaco, S., Barth, A., Seidel, C. A. M., and Mély, Y. (2021) Fundamental photophysics of isomorphous and expanded fluorescent nucleoside analogues. *Chemical Society Reviews* **50**, 7062-7107
30. Liebert, K., Hermann, A., Schlickerrieder, M., and Jeltsch, A. (2004) Stopped-flow and Mutational Analysis of Base Flipping by the Escherichia coli Dam DNA-(adenine-N6)-methyltransferase. *Journal of Molecular Biology* **341**, 443-454
31. Berg, O. G., Winter, R. B., and Von Hippel, P. H. (1981) Diffusion-driven mechanisms of protein translocation on nucleic acids. 1. Models and theory. *Biochemistry* **20**, 6929-6948
32. von Hippel, P. H., and Berg, O. G. (1989) Facilitated target location in biological systems. *Journal of Biological Chemistry* **264**, 675-678
33. Kuzmič, P. (2009) Chapter 10 - DynaFit—A Software Package for Enzymology. in *Methods in Enzymology* (Johnson, M. L., and Brand, L. eds.), Academic Press. pp 247-280
34. Allan, B. W., Beechem, J. M., Lindstrom, W. M., and Reich, N. O. (1998) Direct Real Time Observation of Base Flipping by the EcoRI DNA Methyltransferase. *Journal of Biological Chemistry* **273**, 2368-2373
35. Gowher, H., and Jeltsch, A. (2000) Molecular enzymology of the Eco RV DNA-(adenine-N6)-methyltransferase: kinetics of DNA binding and bending, kinetic mechanism and linear diffusion of the enzyme on DNA11 Edited by J. Karn. *Journal of Molecular Biology* **303**, 93-110
36. Hamdane, D., Guelorget, A., Guérineau, V., and Golinelli-Pimpaneau, B. (2014) Dynamics of RNA modification by a multi-site-specific tRNA methyltransferase. *Nucleic Acids Res* **42**, 11697-11706
37. Goh, B. C., Xiang, X., Lescar, J., and Dedon, P. C. Crystal structure and functional analysis of mycobacterial erythromycin resistance methyltransferase Erm38 reveals its RNA binding site. *Journal of Biological Chemistry*
38. Michalak, E. M., Burr, M. L., Bannister, A. J., and Dawson, M. A. (2019) The roles of DNA, RNA and histone methylation in ageing and cancer. *Nature Reviews Molecular Cell Biology* **20**, 573-589
39. Raposo, A. E., and Piller, S. C. (2018) Protein arginine methylation: an emerging regulator of the cell cycle. *Cell Division* **13**, 3
40. Zaccara, S., Ries, R. J., and Jaffrey, S. R. (2019) Reading, writing and erasing mRNA methylation. *Nature Reviews Molecular Cell Biology* **20**, 608-624
41. Kawa, I. A., Masood, A., Amin, S., Mustafa, M. F., and Rashid, F. (2019) Chapter 2 - Clinical Perspective of Posttranslational Modifications. in *Protein Modificomics* (Dar, T. A., and Singh, L. R. eds.), Academic Press. pp 37-68
42. Covelo-Molares, H., Bartosovic, M., and Vanacova, S. (2018) RNA methylation in nuclear pre-mRNA processing. *Wiley Interdiscip Rev RNA* **9**, e1489-e1489
43. Yue, Y., Liu, J., and He, C. (2015) RNA N6-methyladenosine methylation in post-transcriptional gene expression regulation. *Genes & Development* **29**, 1343-1355

44. Geiman, T. M., and Robertson, K. D. (2002) Chromatin remodeling, histone modifications, and DNA methylation—how does it all fit together? *Journal of Cellular Biochemistry* **87**, 117-125
45. Arenz, S., Ramu, H., Gupta, P., Berninghausen, O., Beckmann, R., Vázquez-Laslop, N., Mankin, A. S., and Wilson, D. N. (2014) Molecular basis for erythromycin-dependent ribosome stalling during translation of the ErmBL leader peptide. *Nature Communications* **5**, 3501
46. Kerppola, T. K. (2009) Polycomb group complexes—many combinations, many functions. *Trends Cell Biol* **19**, 692-704
47. Moritz, L. E., and Trievel, R. C. (2018) Structure, mechanism, and regulation of polycomb-repressive complex 2. *J Biol Chem* **293**, 13805-13814
48. Takeshita, K., Suetake, I., Yamashita, E., Suga, M., Narita, H., Nakagawa, A., and Tajima, S. (2011) Structural insight into maintenance methylation by mouse DNA methyltransferase 1 (Dnmt1). *Proceedings of the National Academy of Sciences* **108**, 9055
49. Frauer, C., and Leonhardt, H. (2011) Twists and turns of DNA methylation. *Proceedings of the National Academy of Sciences* **108**, 8919
50. Lee, T. T., Agarwalla, S., and Stroud, R. M. (2005) A Unique RNA Fold in the RumA-RNA-Cofactor Ternary Complex Contributes to Substrate Selectivity and Enzymatic Function. *Cell* **120**, 599-611
51. Alian, A., Lee, T. T., Griner, S. L., Stroud, R. M., and Finer-Moore, J. (2008) Structure of a TrmA–RNA complex: A consensus RNA fold contributes to substrate selectivity and catalysis in methyltransferases. *Proceedings of the National Academy of Sciences* **105**, 6876
52. Trixl, L., and Lusser, A. (2019) The dynamic RNA modification 5-methylcytosine and its emerging role as an epitranscriptomic mark. *WIREs RNA* **10**, e1510
53. Matthews, M. M., Thomas, J. M., Zheng, Y., Tran, K., Phelps, K. J., Scott, A. I., Havel, J., Fisher, A. J., and Beal, P. A. (2016) Structures of human ADAR2 bound to dsRNA reveal base-flipping mechanism and basis for site selectivity. *Nat Struct Mol Biol* **23**, 426-433
54. Stephan, N. C., Ries, A. B., Boehringer, D., and Ban, N. (2021) Structural basis of successive adenosine modifications by the conserved ribosomal methyltransferase KsgA. *Nucleic Acids Res* **49**, 6389-6398
55. Singh, J., Raina, R., Vinothkumar, K. R., and Anand, R. (2022) Decoding the Mechanism of Specific RNA Targeting by Ribosomal Methyltransferases. *ACS Chemical Biology* **17**, 829-839
56. Srivatsan, S. G., and Tor, Y. (2007) Synthesis and enzymatic incorporation of a fluorescent pyrimidine ribonucleotide. *Nature Protocols* **2**, 1547-1555
57. Van Der Spoel, D., Lindahl, E., Hess, B., Groenhof, G., Mark, A. E., and Berendsen, H. J. C. (2005) GROMACS: Fast, flexible, and free. *Journal of Computational Chemistry* **26**, 1701-1718
58. Tribello, G. A., Bonomi, M., Branduardi, D., Camilloni, C., and Bussi, G. (2014) PLUMED 2: New feathers for an old bird. *Computer Physics Communications* **185**, 604-613
59. D.A. Case, H. M. A., K. Belfon, I.Y. Ben-Shalom, S.R. Brozell, D.S. Cerutti, T.E. Cheatham, III, V.W.D. Cruzeiro, T.A. Darden, R.E. Duke, G. Giambasu, M.K. Gilson, H. Gohlke, A.W. Goetz, R. Harris, S. Izadi, S.A. Izmailov, C. Jin, K. Kasavajhala, M.C. Kaymak, E. King, A. Kovalenko, T. Kurtzman, T.S. Lee, S. LeGrand, P. Li, C. Lin, J. Liu, T. Luchko, R. Luo, M. Machado, V. Man, M. Manathunga, K.M. Merz, Y. Miao, O. Mikhailovskii, G. Monard, H. Nguyen, K.A. O'Hearn, A. Onufriev, F. Pan, S. Pantano, R. Qi, A. Rahnamoun, D.R. Roe, A. Roitberg, C. Sagui, S. Schott-Verdugo, J. Shen, C.L. Simmerling, N.R. Skrynnikov, J. Smith, J. Swails, R.C. Walker, J. Wang, H. Wei, R.M. Wolf, X. Wu, Y. Xue, D.M. York, S. Zhao, and P.A. Kollman. (2021) Amber 2021, . *University of California, San Francisco*.
60. Barducci, A., Bussi, G., and Parrinello, M. (2008) Well-Tempered Metadynamics: A Smoothly Converging and Tunable Free-Energy Method. *Physical Review Letters* **100**, 020603

FIGURE LEGENDS

Scheme 1: Schematic representation of methylation reaction

Scheme 2: Proposed kinetic model for recognition mechanism adopted by Erm

TABLE 1: Rate constants obtained using stopped-flow measurements

Figure 1. Methylation studies with RNA templates highlighting the importance of bulge sites. (A) RNA sequences tested for methylation activity. ★ indicates deletion. The target base A2058 is highlighted in red. **(B)** In-vitro methylation assay using ³H-SAM. For comprehensive understanding, additional data are added, * are adapted from ref. 23. For A2060C/G/U construct, adenine was mutated either to C, G or U at a time. All of these mutations gave negligible activity. Representative data for A2060C is plotted.

Figure 2. Binding studies with Erm. Normalized anisotropy titration curves **(A)** in the absence and **(B)** in presence of SAM. Solid lines correspond to the fits of the data points to equation 1. The binding constants (K_d) are given in the inset. The plotted anisotropy values are normalized to the maximum value for each curve.

Figure 3. Conformation changes at A2058 and distal bases. Fluorescence spectra of **(A)** 2Ap2058, **(B)** 2Ap2054, **(C)** 2Ap2614, **(D)** thG2057 and **(E)** thG2061. Black, red (or blue) spectra represent free RNA and RNA+ Erm, respectively. The target base A2058 is colored pink. The concentration of Erm chosen (4 μ M) ensured maximum binding. **(F)** Stopped-flow traces for the reaction of 1 μ M 2Ap2054 or 2Ap2058 with 4 μ M Erm in the presence and absence of sinefungin (500 μ M). The 2Ap fluorescence was followed above 320 nm with excitation at 315 nm. The progress curves were analyzed with the Dynafit software using the three-step model in scheme 2 to recover the kinetic parameters indicated in the text. The data supports a plausible base flipping at a target site and highlights the significant changes at sites distal to the target bases where a substantial change in the local environment is noted.

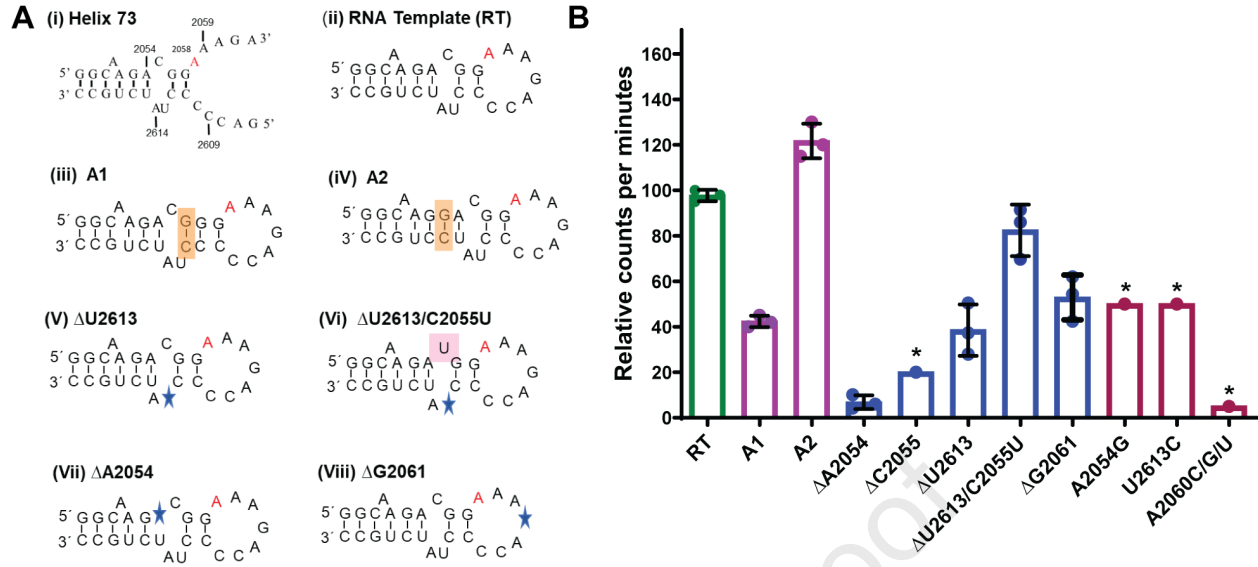
Figure 4: Conformational dynamics of Erm - mini RNA complex. Cartoon representation of Erm-RNA model before **(A)** and after flipping **(B)** of A2058. A double flip mode of interaction of mini-RNA with protein is observed as a predominant mechanism of recognition via MD. The conserved loop1 and loop 12 are colored orange. **(C)** A plot of inter-base distance for the single-stranded RNA in the free and protein-bound forms. The largest changes in the inter-base distances were seen at bases 2054, 2058, 2061, and 2614. **(D)** Free energy surface (FES) for the flipping of A2058. The white dashed line is the minimum free energy path for the base flipping process.. Zoomed view of active site pocket and positioning of A2058 in the model RNA-Erm complex during the MD trajectory **(E)** and crystal structure of taqI DNA Mtase (PDB ID: 1G38) **(F)**. Both show comparable geometry of binding with the mode of the binding being analogous.

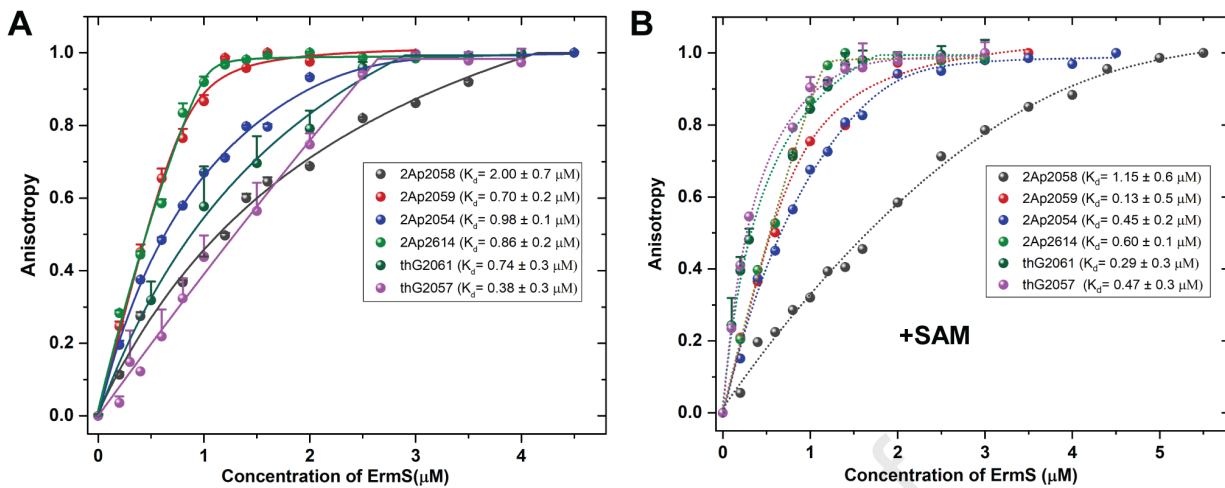
Figure 5: Changes in the RNA conformation during the base flipping event. (A) & (B) Conformational changes in nucleobases close to loop 12 (A2054 and 2614) that lead to a semi-open state. Major structural re-arrangement occurs in this region in the presence of Erm, as reflected by the increase in distance between previously stacked bases. **(C)** Stick representation of the binding site of U2613. **(D)** Surface representation highlighting the groove that U2613 binds.

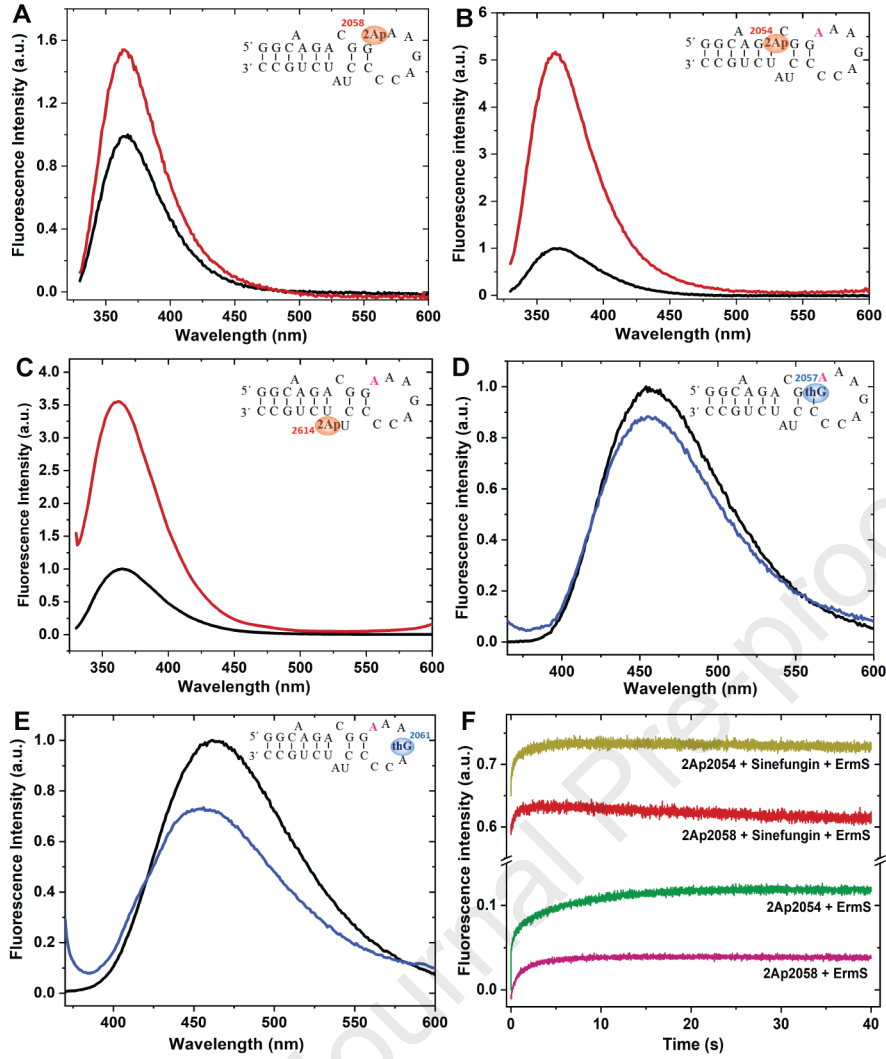
Figure 6: Structural comparison depicting interactions and conformational changes associated with flipping out of target bases in various Mtases. (A) Model structure of Erm-RNA complex. Auxiliary bases help in the anchoring of Erm to its target site by interacting with conserved loops. **(B)** Structure of RumA-RNA complex. The binding of RumA triggers the flipping of the secondary base that interacts with the cofactor. **(C)** Structure of Nsun6 in complex with tRNA. Comparison of RNA conformation before and after flipping of target base: **(D)** Superposition of h73 obtained from simulation before and after flipping of A2058 and **(E)** RumA rRNA substrate architecture before and after binding to protein. **(F)** Structure of 30S-ribosome KsgA complex. G1516 flipping helps in the proper positioning of target bases A1518 and A1519

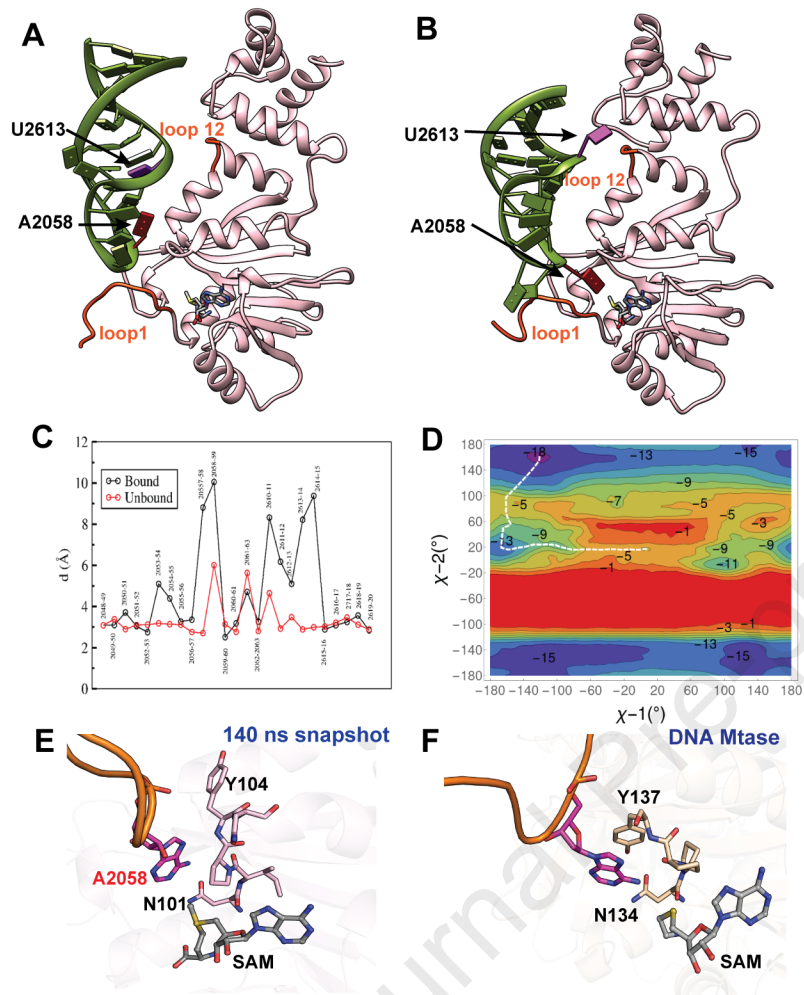
Journal Pre-proof

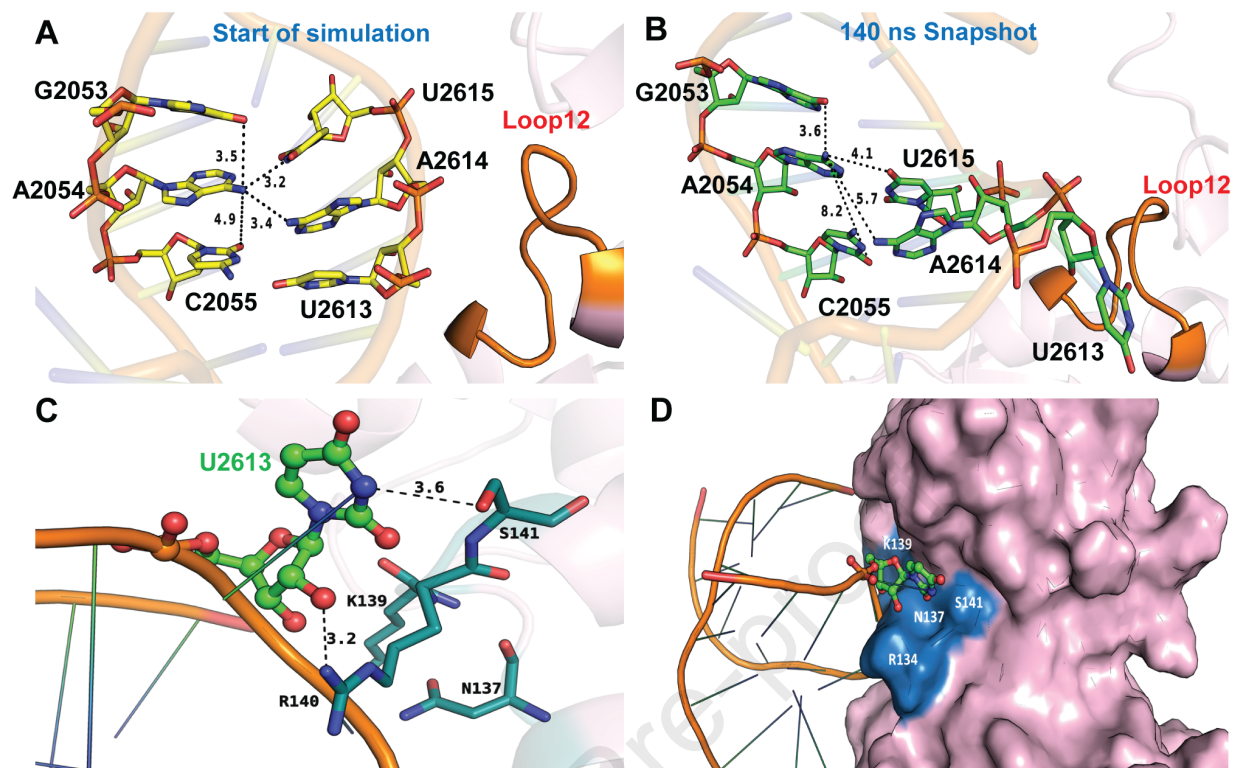
Construct	k_1 ($M^{-1} s^{-1}$)	k_{-1} (s^{-1})	k_2 (s^{-1})	k_3 (s^{-1})
2Ap2058	$5.0 \pm 0.4 \times 10^6$	32 ± 2	3.4 ± 0.5	0.19 ± 0.01
2Ap2058+ Sinefungin	$> 10^8$	32 (fixed)	1.9 ± 0.8	< 0.01
2Ap2054	$2.1 \pm 0.2 \times 10^7$	69 ± 5	2.3 ± 0.1	0.12 ± 0.01
2Ap2054+ Sinefungin	$> 10^8$	69 (fixed)	1.1 ± 0.4	--

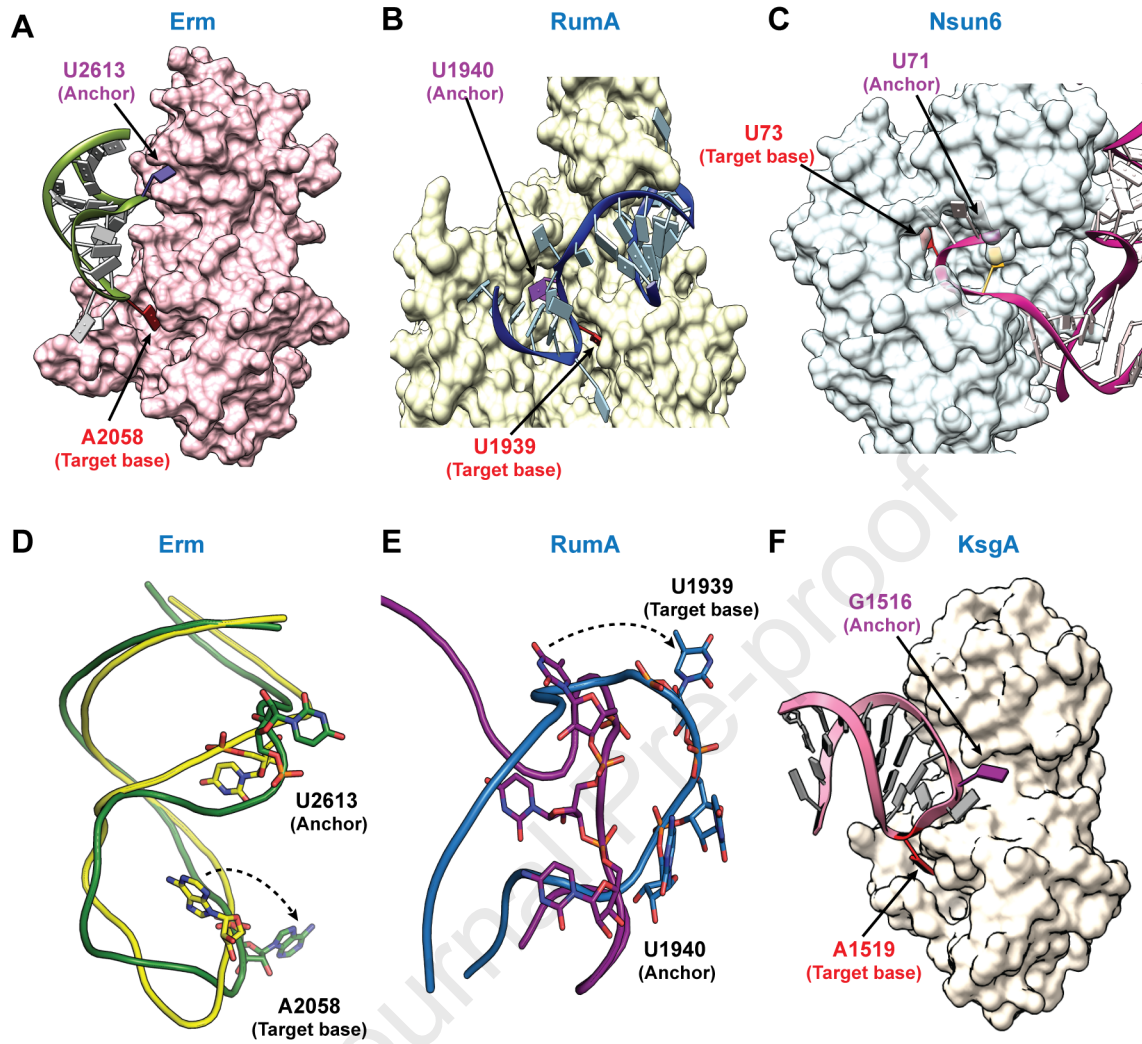


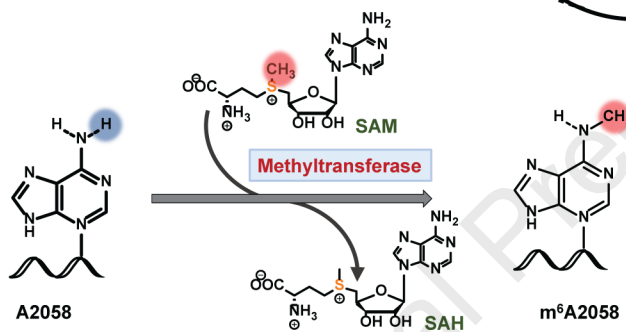
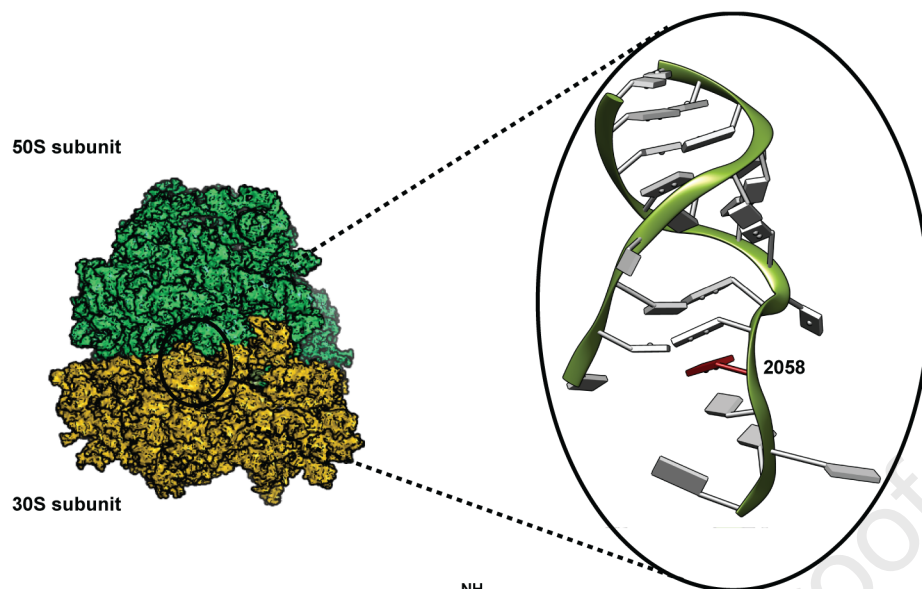


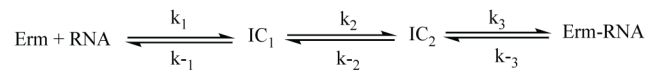












Journal Pre-proof

Author credit statement

Ruchika Bhujbalrao: Visualisation, Investigation, Methodology **Krishna Gavvala:** Investigation (fluorescence experiments) **Reman Kumar Singh:** Investigation (molecular dynamic studies) **Juhi Singh** (UV melting and MALDI) **Christian Boudier:** Formal analysis **Sutapa Chakrabarti:** Writing- Reviewing and Editing **G. Naresh Patwari:** Writing- Reviewing and Editing **Yves Mély:** Supervision, Resources, Writing - Original Draft **Ruchi Anand:** Conceptualization, Supervision, Resources, Writing - Original Draft

Journal Pre-proof